NeuroImage 98 (2014) 1–10

Contents lists available at ScienceDirect

NeuroImage

journal homepage: www.elsevier.com/locate/ynimg

Network-dependent modulation of brain activity during sleep

Takamitsu Watanabe [a,b,*], Shigeyuki Kan [c], Takahiko Koike [c], Masaya Misaki [c], Seiki Konishi [a], Satoru Miyauchi [c], Yasushi Miyahsita [a], Naoki Masuda [d,**]

[a] Department of Physiology, The University of Tokyo, School of Medicine, Tokyo, 113–0033, Japan
[b] Institute of Cognitive Neuroscience, University College London, London, WC1N 3AR, UK
[c] Advanced ICT Research Institute, National Institute of Information and Communications Technology, Hyogo, 651–2492, Japan
[d] Department of Mathematical Informatics, The University of Tokyo, Tokyo, 113–8656, Japan

ARTICLE INFO

Article history:
Accepted 29 April 2014
Available online 9 May 2014

ABSTRACT

Brain activity dynamically changes even during sleep. A line of neuroimaging studies has reported changes in functional connectivity and regional activity across different sleep stages such as slow-wave sleep (SWS) and rapid-eye-movement (REM) sleep. However, it remains unclear whether and how the large-scale network activity of human brains changes within a given sleep stage. Here, we investigated modulation of network activity within sleep stages by applying the pairwise maximum entropy model to brain activity obtained by functional magnetic resonance imaging from sleeping healthy subjects. We found that the brain activity of individual brain regions and functional interactions between pairs of regions significantly increased in the default-mode network during SWS and decreased during REM sleep. In contrast, the network activity of the fronto-parietal and sensory-motor networks showed the opposite pattern. Furthermore, in the three networks, the amount of the activity changes throughout REM sleep was negatively correlated with that throughout SWS. The present findings suggest that the brain activity is dynamically modulated even in a sleep stage and that the pattern of modulation depends on the type of the large-scale brain networks.

Introduction

Sleep consists of characteristic stages: rapid eye movement (REM) sleep and non-REM (NREM) sleep (Cirelli and Tononi, 2008; Diekelmann et al., 2011; Spoormaker et al., 2011; Wang et al., 2011). REM sleep is characterized by rapid eye movements, muscle paralysis, and low-voltage irregular electro-encephalography (EEG) that is similar to those observed during wakefulness. NREM sleep is further divided into light and deep NREM sleep, and the latter is characterized by high-voltage synchronized slow EEG (Aserinsky and Kleitman, 1953; Diekelmann et al., 2011; Wang et al., 2011). In particular, the part of deep NREM sleep in which EEG is the most synchronized is referred to as slow-wave sleep (SWS). The different types of sleep are considered to affect brain activity differently and to play distinct roles in a variety of cognitive functions (Aserinsky and Kleitman, 1953; Diekelmann and Born, 2010; Hobson and Pace-Schott, 2002; Tononi and Cirelli, 2003, 2006).

Prior studies found characteristic modulations of regional brain activity during different sleep stages. During SWS sleep, a part of the hippocampal network is reactivated if the network is activated during preceding wakefulness (Diekelmann and Born, 2010; Diekelmann et al., 2011; Ji and Wilson, 2007; Nir et al., 2011; Peigneux et al., 2004; Wilson and McNaughton, 1994). During REM sleep periods, hippocampal activity in rats is considered to be reduced and normalized (Grosmark et al., 2012).

These changes in local neural activity within a sleep stage play an essential but not exclusive role in functions of sleep such as memory maintenance and homeostasis; modulation of functional interactions among brain regions is also needed (Diekelmann and Born, 2010; Tononi and Cirelli, 2006). In fact, previous human neuroimaging studies compared functional connectivity patterns between wakefulness and sleep periods such as NREM sleep (Andrade et al., 2011; Horovitz et al., 2009; Koike et al., 2011; Sämann et al., 2011; Spoormaker et al., 2012), sleep stage 1 (Horovitz et al., 2008; Larson-Prior et al., 2009, 2011; Spoormaker et al., 2012; Uehara et al., 2013; van Dongen et al., 2011), SWS (Chow et al., 2013; Koike et al., 2011; Spoormaker et al., 2012), and REM sleep (Chow et al., 2013; Laureys et al., 2001; Maquet et al., 2000). Nevertheless, to compare the connectivity across different types of sleep stages, these neuroimaging studies implicitly assumed that functional connectivity was stable during a given sleep stage. Therefore, although some observations have been made for microscopic changes within sleep periods (Grosmark et al., 2012), modulation of

* Correspondence to: T. Watanabe, Institute of Cognitive Neuroscience, University College London, 17 Queen Square, London, WC1N 3AR, UK.
** Correspondence to: N. Masuda, Department of Mathematical Informatics, The University of Tokyo, 7-3-1 Hongo, Bunkyo-ku, Tokyo, 113–8656, Japan.
E-mail addresses: takamitsu.watanabe@ucl.ac.uk (T. Watanabe), masuda@mist.i.u-tokyo.ac.jp (N. Masuda).

http://dx.doi.org/10.1016/j.neuroimage.2014.04.079
1053-8119/

large-scale functional interactions within a sleep stage has not been clarified.

In the present study, we investigated modulation of inter-regional functional interactions within SWS and REM sleep periods by looking at the resting-state networks (RSNs). Neuroimaging studies have indicated that brain regions tightly interact with each other during rest and constitute several large-scale brain networks, known as the RSNs (Biswal et al., 1995; Dosenbach et al., 2006; Fair et al., 2009; Greicius et al., 2003; Raichle et al., 2001). The RSNs are involved in various cognitive functions. For example, the default-mode network (DMN) consists of brain regions that are considered to be recruited for maintenance of long-term memory (Buckner et al., 2008; Greicius et al., 2003; Raichle et al., 2001; Uddin et al., 2009). The fronto-parietal network (FPN) consists of regions that are considered to be used in attentional cognitive tasks (Dosenbach et al., 2006; Fair et al., 2009).

Hinted by these findings on different types of RSNs and the aforementioned observations on changes in local neural activity during sleep, we hypothesized that, at a macroscopic level, different RSNs may show different modulation patterns in functional connectivity within SWS and REM sleep periods. For example, the functional interactions in the DMN may increase in SWS periods and decrease in REM sleep because the hippocampal activity, which is tightly related to long-term memory, shows the same pattern (Diekelmann et al., 2011; Diekelmann and Born, 2010; Grosmark et al., 2012; Ji and Wilson, 2007; Peigneux et al., 2004; Wilson and McNaughton, 1994). The functional interactions in the FPN may show the opposite pattern of modulation because the local neural activity in the fronto-parietal areas is reduced during SWS periods (Huber et al., 2004, 2006; Nir et al., 2011).

Technically, functional magnetic resonance imaging (fMRI) allows us to record activity from the entire human brain. The recorded activity does not directly reflect neural activity such as neural spikes, but is highly correlated with local-field potentials of neurons (Logothetis et al., 2001). However, the conventional analysis method based on Pearson's correlation coefficient (Biswal et al., 1995; Fair et al., 2009; Greicius et al., 2003; Honey et al., 2009; Uddin et al., 2009) has not reported significant changes in functional interactions within SWS and REM sleep. This limitation of the correlation-based method may result from its susceptibility to spurious correlation induced by common neighbors of two brain areas (Adachi et al., 2012).

Here, we examine the modulation of functional interactions in the human RSNs throughout SWS and REM sleep by applying the so-called pairwise maximum entropy model (MEM) (Roudi et al., 2009; Schneidman et al., 2006; Shlens et al., 2006; Tang et al., 2008; Watanabe et al., 2013). In contrast to the methods derived by the Pearson's correlation coefficient, the pairwise MEM determines the functional interaction between two brain regions with the consideration of functional interaction between other pairs of regions. Therefore, it would not suffer from pseudo-correlations originating from common neighbors of two brain regions. In fact, the pairwise MEM accurately and robustly describes activity in the large-scale human brain networks during rest and captures more anatomical and physiological information than conventional methods do (Watanabe et al., 2013). We exploited these advantages of the pairwise MEM to examine the "macroscopic network-dependent activity change" hypothesis.

Materials and methods

Data acquisition

We used almost the same data set as that used in our previous study (Koike et al., 2011). The data set consists of fMRI signals, EEG, and videos of eye movements, which were simultaneously recorded while 14 healthy subjects (12 males and 2 females; mean age, 25 years) were sleeping inside an MRI scanner. The data obtained from 12 of the 14 subjects were recorded for our previous study (Koike et al., 2011), and those obtained from the other two subjects were subsequently added for the present study. The 12 subjects participated in this experiment twice (i.e., two nights) with an interval larger than two weeks. The other two subjects participated once. In total, we obtained approximately 95 h of the data, which extended over 26 nights (Table S3). The recording procedure was approved by the ethics committee of the National Institute of Information and Communications Technology Japan and was in accordance with the Declaration of Helsinki. All the subjects provided written informed consent before the recording.

All the subjects had regular sleep–wake cycles according to their self-report and did not have a history of any neurological, psychiatric, or endocrine disorder. None of them took any medication. Ingestion of alcohol and caffeine was not allowed from 24 h before the start of the recording to the end of the experiment. To obtain a sufficient length of SWS and REM periods from each subject, the subjects were made accustomed to sleeping in a noisy fMRI scanner as follows: They were asked to listen to noise that had been recorded in previous fMRI scanning at least two hours per day in the two days before the experiment. On the day before the fMRI scanning, the subjects slept in a fMRI scanner in the presence of the previously recorded noise, whereas their brains were not scanned. On the day of the fMRI scanning, the subjects were not allowed to sleep until the scanning began between 3:00 AM and 6:00 AM. The subjects then wore earplugs and soundproof headsets and slept inside the fMRI scanner. These preparations urged the subjects to sleep continuously and long in the fMRI scanner.

We recorded fMRI data using a 1.5 T MRI scanner (MAGNETOM Vision plus, Siemens, Germany). T1-weighted images were acquired for anatomical reference (3D MPRAGE, 1 mm^3). fMRI images were obtained in accordance with gradient echo single-shot EPI sequence (24 slices, $4 \times 4 \times 5$ mm^3 resolution, TR = 4 s, TE = 55 ms, flip angle = 90°). An fMRI scan took 55 min and was repeated until the subjects became completely awake or expressed discomfort.

We recorded EEG concurrently with the fMRI scanning using an MRI-compatible amplifier (BrainAmp MR, Brain Products GmbH, Germany) and a 24-channel electrode cap with Ag/AgCl ring electrodes (Falk Minow Services, Germany). A reference electrode was located at the midpoint between Fz and Cz (impedance <3 kΩ). We filtered the EEG data at 0.016 − 250 Hz, sampled them at 5000 Hz using Brain Vision Recorder (Brain Products GmbH, Germany) and conducted offline correction of scanning and ballistocardiogram artifacts using Brain Vision Analyzer software (Brain Products GmbH, Germany). We adopted a "template drift compensation" method to correct for gradient-induced artifacts and a "template matching" method to correct for cardioballistic artifacts, both of which were implemented in Brain Vision Analyzer. As a standard polysomnography protocol, electromyographic (EMG) and electrooculographic (EOG) recordings were also conducted.

Definition of sleep periods

Using the EEG, EMG, and EOG data, a trained psychiatrist (TW) scored sleep stages for each 30-s interval in accordance with the international criteria (Rechtschaffen and Kales, 1968). On the basis of the scores, we defined sleep stages 1, 2, 3, 4, and REM sleep. SWS was defined as the union of sleep stages 3 and 4 (Rechtschaffen and Kales, 1968). We discarded SWS and REM periods shorter than 12 min.

We defined P1/P2/P3 SWS and P1/P2/P3 REM as follows (Fig. 1A): P1/P2/P3-SWS/REM were derived from the first 36 min of SWS/REM periods. P1 comprised the first 12 min of each sleep period. P2 comprised the next 12 min. P3 was defined similarly. The combined lengths of P1, P2, and P3 were not all identical because some SWS and REM periods lasted less than 36 min. We also defined Pre and Post period of SWS/REM as 12-min period right before and after a SWS/REM sleep period, respectively. When a tentative Pre/Post period overlapped with another time window (i.e., P1/P2/P3 or tentative Pre/Post), we discarded the tentative Pre/Post period. The total length of P1/P2/P3/Pre/Post SWS/REM collected over all subjects ranged between approximately 7 h and 10 h (Table S3).

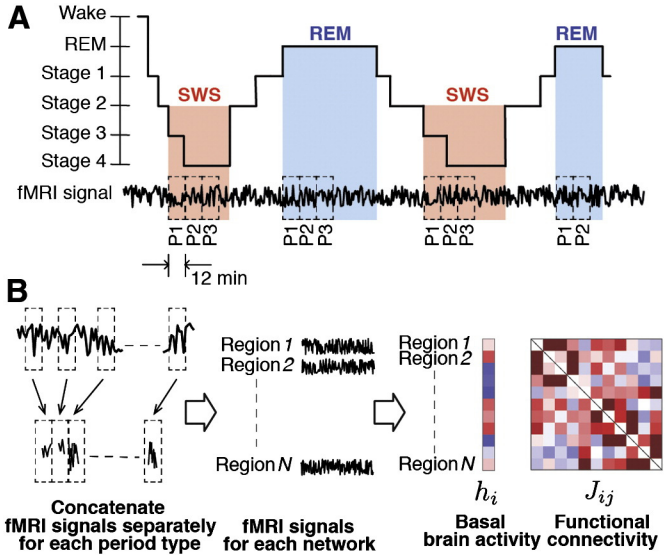

Fig. 1. Flow of the data analysis. A. On the basis of EEG, we first determined sleep stages including SWS periods and REM periods. The preprocessed fMRI signals surrounding sleep periods were classified into the following six signal groups: P1/P2/P3-SWS and P1/P2/P3-REM. Each group was defined by a time window of 12 min. For each group, the fMRI signals recorded at different time points and for different subjects were combined. Because SWS and REM periods can be shorter than 36 min, the total length of the fMRI signals depends on the signal group. B. We focused on fMRI signals in the N brain regions belonging to each RSN (i.e., DMN and FPN). We fitted the pairwise MEM to the fMRI data at the N regions to infer the basal brain activity, h_i, and functional connectivity, J_{ij}, for each RSN and each signal group.

A short time window enables us to track dynamical changes in the network activity with a high temporal resolution. However, the fitting accuracy of the pairwise MEM decreases as the time window is shortened. With the time window of 10 min, the fitting accuracy was low. With the time window of 15 min, the amount of data for P3, i.e., those between 30 and 45 min since the initiation of SWS or REM sleep, was insufficient. By taking into account the trade-off, we set the length of the time window to 12 min.

Preprocessing of fMRI data

In accordance with previous fMRI studies on brain activity during resting or sleep states (Honey et al., 2009; Kaufmann et al., 2006; Uddin et al., 2009; Watanabe et al., 2013), we preprocessed the fMRI data in SPM8 (www.fil.ion.ucl.ac.uk/spm/). For each scanning session and each subject, the fMRI images underwent realignment, slice-timing correction, and normalization to the standard template image (ICBM 152). After temporal band-pass filtering (0.01–0.1 Hz) with in-house MATLAB scripts, the images underwent spatial smoothing (full-width half maximum = 8 mm) in SPM8. The images were then combined for each subject and corrected for his/her head motion, whole-brain signals, ventricular signals, white matter signals, and the run effect. Using CORSICA (McKeown et al., 1998), we reduced noise related to respiration and heart beat.

Regarding the correction for the whole-brain signals, we should note that its necessity is still under debate (Hayasaka, 2013; van Dijk et al., 2010). In fact, there is no clear consensus about what portion of the whole-brain signals represents physiological noise (Birn et al., 2006; Chang and Glover, 2009a; Wise et al., 2004) or neural activity (Schölvinck et al., 2010). Therefore, it is also unclear whether or not we should correct the effect of the global signals: a study stated that regressing out of the whole-brain signals could induce spurious negative correlations (Murphy et al., 2009), and another study reported that negative correlations between different RSNs were only observed when global-signal regression was adopted (Weissenbacher et al., 2009); on the other hand, others showed that some of such negative correlations were observed even without a global-signal regression process, though they also stated that we should refrain from interpreting the negative correlation coefficients (Chang and Glover, 2009b; Fox et al., 2009). Considering these debates, alternative methods such as a type of a principle component analysis (Behzadi et al., 2007) are increasingly adopted (Chai et al., 2012). In the present study, although we also observed that the global-signal regression negatively shifted the correlation coefficients (Fig. S10), we adopted the simple conventional regression method and corrected the global signal, because we focused on the changes in the functional interaction and aimed at avoiding overestimation of the magnitude of the interactions.

Owing to slow and long-lasting hemodynamic reactions, fMRI images recorded at adjacent time points are strongly correlated, which can adversely affect the MEM analysis (Roudi et al., 2009). We reduced this correlation using a general linear model as follows: if the data for a given subject consisted of T images, we built T regressors whose onset was set to the start time of each image acquisition. After convolving the regressors with a hemodynamic response function implemented in SPM 8, we estimated regression coefficients, which are thought to represent brain activity at each time point of data acquisition.

We then extracted fMRI signals that belonged to either of the ten signal groups of sleep-related periods. The extracted signals were averages over a sphere of 4-mm in radius whose center was located at the anatomical coordinates of a brain region in the DMN or FPN (Table S1). Same as a prior study that investigated the organization of the RSNs (Fair et al., 2009), the locations of the brain regions in each RSN (i.e., 12 regions for the DMN and 11 regions for the FPN) were determined by a previous meta-analysis (Dosenbach et al., 2006, Table S1). For the DMN, an independent component analysis (ICA) of the present data also identified a group of brain regions (Table S2) that were similar to the previously reported regions (Dosenbach et al., 2006, Table S1). Although our hypothesis pertaining to the DMN is partly based on the previous findings on hippocampal activity (Diekelmann et al., 2011; Diekelmann and Born, 2010; Grosmark et al., 2012; Ji and Wilson, 2007; Peigneux et al., 2004; Wilson and McNaughton, 1994), we did not add the hippocampus to the DMN because the hippocampus is close to the parahippocampal gyrus, a region already included in the DMN, and the ICA did not detect the hippocampus.

Fitting of the pairwise MEM

We fitted the pairwise MEMs to the preprocessed fMRI data in essentially the same manner as in our previous study (Watanabe et al., 2013). To normalize the signals in each signal group, we subtracted the average from the signals and then divided the obtained values by their standard deviation. The normalization was conducted at each region. The normalized signals were binarized with a threshold of 0.075, which maximized the accuracy of fit defined in the following. The accuracy of fit was robust with respect to the threshold value ranging from –0.2 to 0.2 (Fig. S2).

The binarized activity at brain region i and discrete time t, denoted by σ_i^t, is either on (+1) or off (0). The network state at time t is represented by $V^t = [\sigma_1^t, \sigma_2^t, \ldots, \sigma_N^t]$, where N is the number of the brain regions in an RSN (i.e., $N = 12$ for the DMN and $N = 11$ for the FPN). The empirical activation probability of region i, denoted by $\langle \sigma_i \rangle$, is equal to $(1/T) \sum_{t=1}^{T} \sigma_i^t$, where T is the number of images in the signal group of interest. The empirical joint activation probability of regions i and j, denoted by $\langle \sigma_i \sigma_j \rangle$, is given by $(1/T) \sum_{t=1}^{T} \sigma_i^t \sigma_j^t$.

To fit the pairwise MEM to the data, we maximized the entropy of the distribution of the network state under the restriction that $\langle \sigma_i \rangle$ and $\langle \sigma_i \sigma_j \rangle$ $(1 \le i \le j \le N)$ for the inferred model are equal to the empirical values. Such a distribution is known to have the form $P(V_k) = e^{-E(V_k)} / \sum_{\ell=1}^{2^N} e^{-E(V_\ell)}$, where $P(V_k)$ is the probability of the k th network state V_k, and $E(V_\ell) = -\sum_{i=1}^{N} h_i \sigma_i(V_\ell) - (1/2) \sum_{i=1}^{N} \sum_{j=1, j \neq i}^{N} J_{ij} \sigma_i(V_\ell)$

$\sigma_j(V_\ell)$. σ_i (V_ℓ) indicates the value of σ_i (i.e., 1 or 0) under network state V_ℓ. The so-called basal brain activity h_i represents the tendency of activation at region i when it is isolated from the other regions. J_{ij} represents the functional interaction between regions i and j. For the inferred model, the expected activation probability, $\langle\sigma_i\rangle_m$, and the expected pairwise joint activation probability, $\langle\sigma_i\sigma_j\rangle_m$, are given by $\langle\sigma_i\rangle_m = \sum_{\ell=1}^{2^N}\sigma_i(V_\ell)P(V_\ell)$ and $\langle\sigma_i\sigma_j\rangle_m = \sum_{\ell=1}^{2^N}\sigma_i(V_\ell)\sigma_j(V_\ell)P(V_\ell)$, respectively. We determined h_i and J_{ij} by iteratively adjusting $\langle\sigma_i\rangle_m$ and $\langle\sigma_i\sigma_j\rangle_m$ toward $\langle\sigma_i\rangle$ and $\langle\sigma_i\sigma_j\rangle$, respectively, with a gradient descent algorithm (Schneidman et al., 2006; Shlens et al., 2006; Tang et al., 2008; Watanabe et al., 2013).

The accuracy of fit quantifies the performance of the pairwise MEM model relative to that of the independent MEM (Roudi et al., 2009; Schneidman et al., 2006; Shlens et al., 2006; Tang et al., 2008; Watanabe et al., 2013; Yeh et al., 2010). The independent MEM is defined as the MEM whose parameters are inferred under the additional restriction that all the pairwise interactions are absent (i.e., $J_{ij} = 0$ for all i and j). For the two types of MEMs, we quantified the discrepancy between the model and data by the Kullback–Leibler distance, D_k (k = 1 and 2 for the independent and pairwise MEMs, respectively), which is given by $D_k = \sum_{\ell=1}^{2^N}P_{data}(V_\ell)\log_2(P_{data}(V_\ell)/P(V_\ell))$, where P_{data} (V_ℓ) is the empirical probability of network state V_ℓ. The accuracy of fit is defined by $r_D = (D_1 - D_2)/D_1$. The r_D value, which ranges between 0 and 1, is large if the model accurately fits the data.

Estimation of functional connectivity by other methods

As controls, we calculated the connection strength between pairs of brain regions using three other methods. The data employed are the same as those used for estimating the pairwise MEM.

First, we estimated the functional connectivity using the Pearson's correlation coefficient. After conducting the same preprocessing and temporal filtering as in the case of the pairwise MEM, we calculated Pearson's correlation coefficients (Biswal et al., 1995; Fair et al., 2009; Greicius et al., 2004; Honey et al., 2009; Uddin et al., 2009) between the brain activities at pairs of regions. We applied the Fisher's transformation to the correlation coefficients, obtained Z values for each subject, and averaged the Z values over the subjects. Then, we compared the absolute Z values among the three time periods (i.e., P1, P2, and P3) separately for SWS and REM.

Second, we estimated the functional connectivity using the partial correlation method (Salvador et al., 2005, 2008). The partial correlation between brain regions i and j, r_{ij}, is given by $r_{ij} = -\Gamma_{ij}^{-1}/\sqrt{\Gamma_{ii}^{-1}\Gamma_{jj}^{-1}}$, where Γ is the covariance matrix for $X_t = [X_1(t), X_2(t), \ldots, X_N(t)]$, the N-dimensional row vector representing the continuous-valued activity at the N regions at time t. We then averaged the r_{ij} value over the subjects and compared the absolute r_{ij} values among the three time periods (i.e., P1, P2, P3) separately for SWS and REM.

Third, we estimated the functional connectivity using the mutual information (MI) method (Salvador et al., 2008, 2010). The MI between brain regions i and j at frequency ω_k is given by $MI_{ij} = (-1/2)\ln(1 - mCoh_{ij}(\omega_k))$, where $mCoh_{ij}(\omega_k)$ indicates the multiple coherence between fMRI signals at regions i and j at frequency ω_k. We then averaged $MI_{ij}(\omega_k)$ across ω_k ($0.01Hz < \omega_k < 0.1$ Hz) to obtain the MI between regions i and j.

Somato-sensory network

To examine the generality of the network-dependent activity change, we calculated changes in activity of the somato-sensory network (SMN) in the same manner as we did for the DMN and FPN. Based on previous studies (Dosenbach et al., 2006; Fair et al., 2009), the regions constituting the SMN were determined (Table S5). The limited amount of the present data forced us to restrict the number of the regions to ten.

Statistical analysis

We tested the difference between the h_i and $|J_{ij}|$ values before and after a sleep period using paired t-tests across regions and region pairs, respectively. Concerns regarding multiple comparisons were solved by calibration of the threshold P value of 0.05 on the basis of Bonferroni corrections among eight possible conditions: two RSNs (DMN and FPN) × two types of sleep (SWS and REM) × two types of network activity (h_i and $|J_{ij}|$). The uncorrected threshold P value is equal to 0.00625.

The modulation of the network activity throughout sleep periods was first tested by the Friedman test with $P < 0.05$, Bonferroni-corrected among the eight possible conditions described above. We then conducted post-hoc tests to examine the difference in the network activity between P1 and the other five periods. To this end, we used the Wilcoxon signed rank test with $P < 0.05$, which was Bonferroni-corrected between the two periods (i.e., P2 and P3).

Results

High fitting accuracy of the pairwise MEM to fMRI signals during sleep

To examine the modulation of network activity throughout the different sleep periods, we defined the six signal groups (P1/P2/P3-SWS and P1/P2/P3-REM; Fig. 1A, see Materials and methods) and gathered fMRI signals recorded from 14 subjects to obtain approximately 7–10 h of signals (Table S3). Using the classified fMRI signals, we then separately fitted the pairwise MEM to each group of fMRI signals, which were recorded at the regions belonging to the DMN and FPN (Fig. 1B, Table S1).

For both brain networks and all the six signal groups, the pairwise MEM realized more than 85% accuracy of fit to the fMRI signals (Table S4, Fig. S1). The accuracy of fit was robust with respect to the threshold for binarization, a parameter used in the fitting procedures (Fig. S2). The fitting procedure provided us with two indicators: h_i, representing the activity at region i when it is hypothetically isolated from the other regions (Fig. 2A), and J_{ij}, representing the functional connectivity between regions i and j (Fig. 2B) (Roudi et al., 2009; Schneidman et al., 2006; Shlens et al., 2006; Watanabe et al., 2013). The estimated values of h_i and J_{ij} were robust with respect to the subjects; the h_i and J_{ij} values obtained from seven randomly selected subjects are almost equal to those obtained from the remaining seven subjects ($r > 0.8$ for all the signal groups; Figs. 2C and D). These results suggest that the pairwise MEM accurately and robustly captures the network activity during sleep.

Changes in network activity throughout SWS and REM periods in the DMN

We then examined the changes in network activity throughout SWS and REM periods in terms of h_i and J_{ij}. Regarding J_{ij}, we tracked the absolute value, which we call the connection strength between regions i and j, because positive and negative J_{ij} values are considered to represent excitatory and inhibitory functional connectivity, respectively (Roudi et al., 2009; Schneidman et al., 2006; Shlens et al., 2006; Watanabe et al., 2013).

In the DMN, significant changes in both the basal brain activity, h_i, and the connection strength, $|J_{ij}|$, were detected throughout both SWS and REM periods (SWS/REM: $F_{(2,\ 22)} = 18.2/22.2$ for h_i and $F_{(2,\ 130)} = 112.8/122.4$ for $|J_{ij}|$, respectively. $P < 0.01$, Friedman test, Bonferroni-corrected). A post-hoc test revealed that the h_i and $|J_{ij}|$ values in P2 and P3 were significantly different from those in P1 (SWS/REM: $z > 3.2/3.3$ for h_i and $z > 7.0/7.1$ for $|J_{ij}|$, respectively. $P < 0.01$, Wilcoxon signed rank tests, Bonferroni-corrected, Figs. 3A and B). In contrast, there was no significant difference between P2 and P3 in both SWS and REM sleep ($P > 0.5$).

Furthermore, for both SWS and REM sleep, h_i and $|J_{ij}|$ in P1 were not different from those calculated from the 12-min data right before P1 ($P > 0.6$, Fig. S3). h_i and $|J_{ij}|$ in P3 were not different from those calculated from the 12-min data right after each sleep period (P3 versus right after each sleep period, $P > 0.7$ in both SWS and REM sleep, Fig. S3). It should be noted that either of the time periods right before P1 or those right

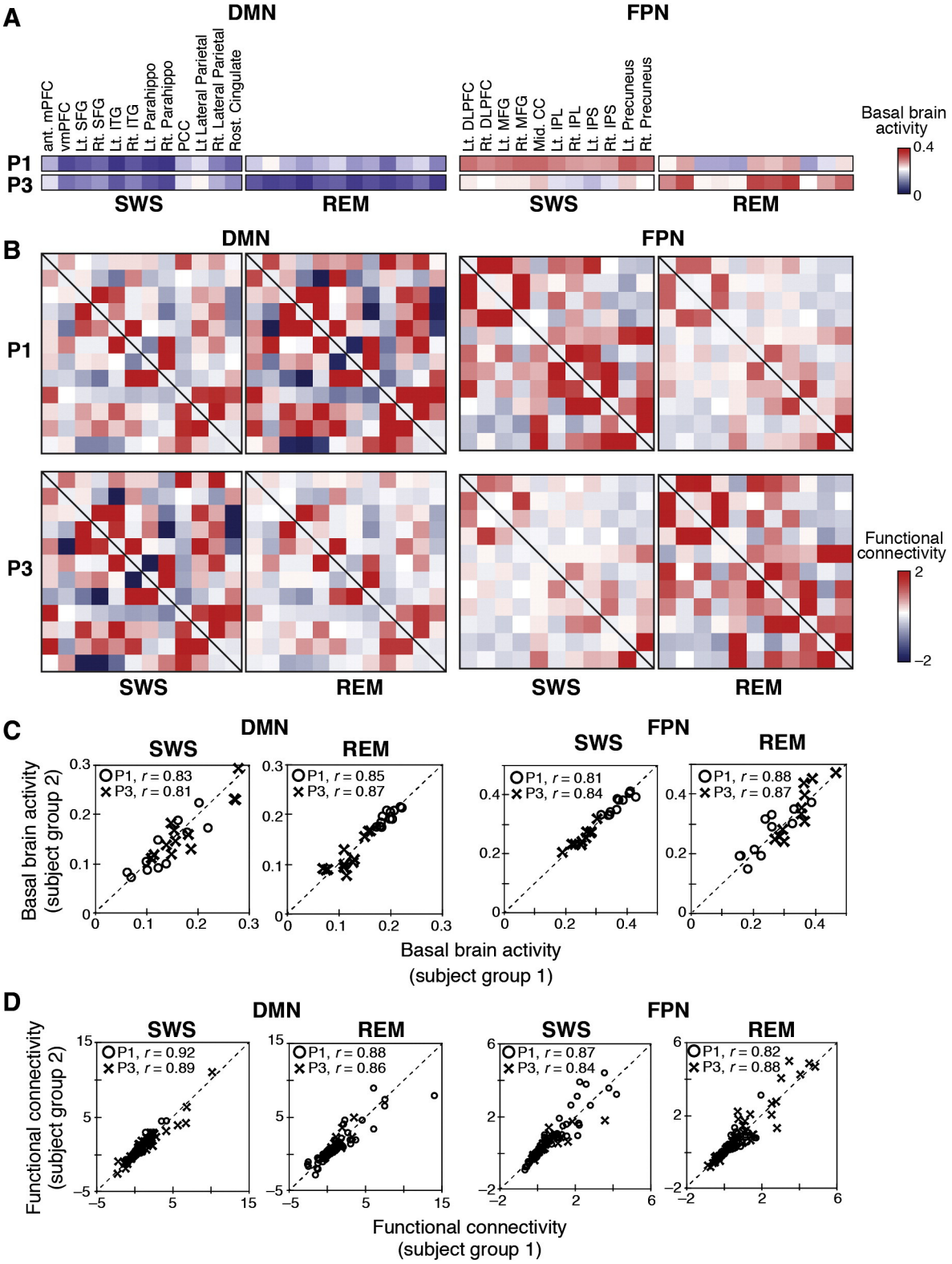

Fig. 2. Basal brain activity and functional connectivity estimated by the pairwise MEM. A. Basal brain activity at each region in the two RSNs in P1 and P3 in the two types of sleep period. The anatomical locations of the brain regions in each RSN were determined based on previous studies (Dosenbach et al., 2006, Table S1). Lt., left; Rt., right; Ant mPFC, anterior medial prefrontal cortex; vmPFC, ventro-medial prefrontal cortex; SFG, superior frontal gyrus; ITG, inferior temporal gyrus; PCC, posterior cingulate cortex; DLPFC, dorsolateral prefrontal cortex; MFG, middle frontal gyrus; Mid CC, middle cingulate cortex; IPL, inferior parietal lobule; IPS, inferior parietal sulcus. B. Functional connectivity for each region pair. The anatomical labels in panel A were also applied to this panel. C and D. Comparison of the basal activity, h_i, and functional connectivity, J_{ij}, obtained from 7 of the 14 subjects (subject group 1) and those obtained from the remaining 7 subjects (subject group 2). A cross represents the h_i value for a brain region. A circle represents the J_{ij} value for a region pair.

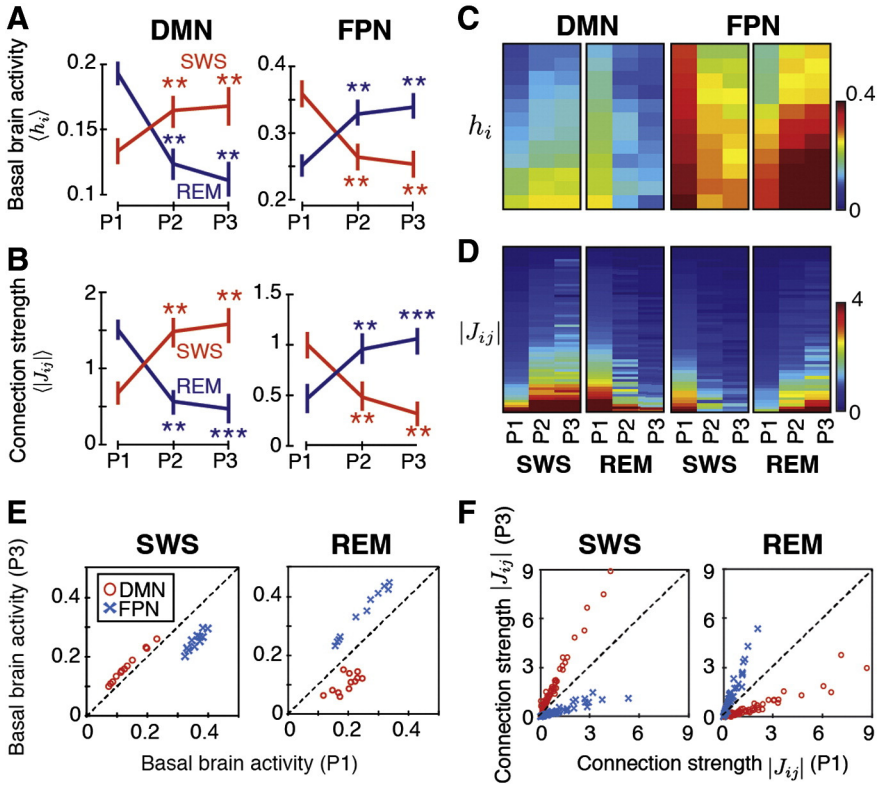

Fig. 3. Time courses of the network activity throughout sleep. A. Averaged basal brain activity in the six 12-min time windows for each RSN and sleep type. ** indicates a significant difference compared with the values at P1 ($P < 0.01$, Bonferroni-corrected). The error bars indicate the standard deviations calculated on the basis of the different brain regions. B. Averaged connection strength in the six 12-min time windows. The error bars indicate the standard deviations calculated on the basis of the different pairs of brain regions. C. Dynamics of the basal activity at the individual brain regions. In each panel, the brain regions are sorted according to the magnitude of the basal activity at the P1-SWS or P1-REM period. D. Dynamics of the connection strength for the individual region pairs. In each panel, the region pairs are sorted according to the magnitude of the connection strength at the P1-SWS or P1-REM period. E. Comparison of the basal brain activity between P1 and P3. F. Comparison of the connection strength between P1 and P3.

after P3 did not overlap with SWS or REM. To summarize, network activity (i.e., h_i and $|J_{ij}|$) in the DMN sharply increased immediately after P1 in SWS, whereas it decreased immediately after P1 in REM sleep. In both cases, the network activity reached a plateau by P3.

Changes in network activity throughout SWS and REM periods in the FPN

In the FPN, we found the opposite patterns. The two indicators representing the network activity significantly changed during sleep periods (SWS/REM: $F_{(2,\ 20)} = 16.2/18.7$ for h_i and $F_{(2,\ 108)} = 99.3/97.8$ for $|J_{ij}|$, respectively, $P < 0.01$, Friedman tests, Bonferroni-corrected). Both h_i and $|J_{ij}|$ values in P1 were significantly larger and smaller than those in the succeeding periods (i.e., P2 and P3) for SWS and REM, respectively (SWS/REM: $z > 3.1/3.3$ for h_i and $z > 6.5/3.8$ for $|J_{ij}|$, respectively, $P < 0.01$, Wilcoxon signed rank tests, Bonferroni-corrected, Figs. 3A and B). Last, as observed in the DMN activity, there was neither significant difference between P1 and the period right before P1 nor between P3 and the period right after each sleep period ($P > 0.7$, Fig. S3).

Sleep-induced changes in activity of individual brain regions and region pairs

The results so far have been derived for the basal brain activity and connection strength averaged over regions and region pairs, respectively. Therefore, the detected modulation may owe to the modulation in a small fraction of regions or region pairs that possess large values of h_i or $|J_{ij}|$. This may be the case in particular because h_i and $|J_{ij}|$ values are heterogeneously distributed, as suggested by Figs. 2A and B. However, this possibility is excluded because individual h_i and $|J_{ij}|$ values were modulated consistently throughout the sleep periods (Figs. 3C and D).

More quantitatively, the h_i values for all the brain regions in the DMN were significantly larger in P3 than in P1 in SWS periods ($t_{(11)} = 31.8$, $P < 3.8 \times 10^{-11}$, paired t test), whereas the opposite was the case for all the brain regions in the FPN ($t_{(10)} = 27.2$, $P < 1.1 \times 10^{-10}$, paired t test; Fig. 3E). In both networks, h_i showed the opposite patterns throughout REM periods. In other words, for all the regions, h_i was significantly larger in P1 than in P3 in REM periods in the DMN ($t_{(11)} = 12.8$, $P < 6.0 \times 10^{-8}$, paired t test), and h_i was significantly larger in P3 than in P1 in REM periods in the FPN ($t_{(10)} = 23.1$, $P < 5.2 \times 10^{-10}$, paired t test; Fig. 3E). The connection strength, $|J_{ij}|$, changed qualitatively in the same pattern as h_i did for all the pairs of regions. In the DMN, it was significantly larger in P3 than in P1 in SWS periods ($t_{(65)} = 7.9$, $P < 3.9 \times 10^{-11}$, paired t test), and it was significantly larger in P1 than in P3 in SWS periods in the FPN ($t_{(54)} = 6.4$, $P < 3.7 \times 10^{-8}$ paired t test; Fig. 3F). In contrast, $|J_{ij}|$ was significantly larger in P1 than in P3 in REM periods in the DMN ($t_{(65)} = 7.3$, $P < 5.7 \times 10^{-10}$, paired t test), and it was significantly larger in P3 than in P1 in REM periods in the FPN ($t_{(54)} = 6.8$, $P < 9.4 \times 10^{-9}$, paired t test; Fig. 3F).

These results support our hypothesis. In the DMN, SWS periods up-regulate both the basal activity and connection strength, whereas REM periods down-regulate these quantities. In the FPN, the two types of sleep period regulate the macroscopic network activity in the opposite directions.

Changes in normalized functional connection strength

In all the cases considered above, sleep periods co-modulated the basal brain activity (h_i) and connection strength ($|J_{ij}|$) in the same direction. If all the h_i and J_{ij} values are scaled by the same factor, the changes can simply be interpreted as the change in just one common parameter,

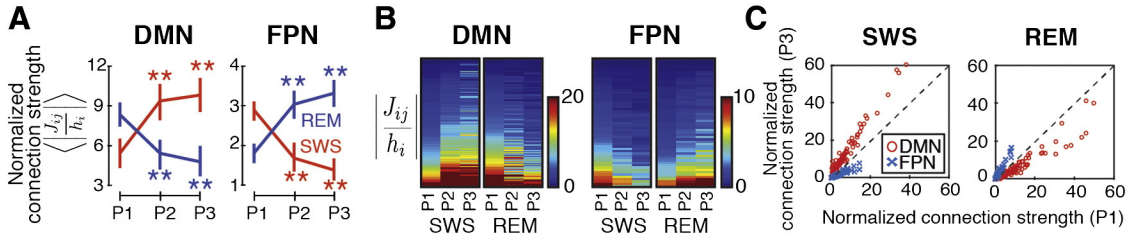

Fig. 4. Time courses of the normalized connection strength throughout sleep. A. Averaged dynamics of the normalized connection strength. B. Dynamics of the normalized connection strength for the individual region pairs. In each panel, the region pairs are sorted according to the magnitude of the normalized connection strength in the P1-SWS or P1-REM period. The number of the region pairs displayed in the figure is twice as large as that in Fig. 3D because there are two normalized connection strength values for each pair of i and j, i.e., $|J_{ij}/h_i|$ and $|J_{ij}/h_j|$. C. Comparison of the normalized connection strength between P1 and P3.

the so-called temperature. In applications of MEMs to condensed matters, for example, a mere change in the temperature does not imply a change in the connectivity within a material. To examine this issue, we measured the dynamics of the normalized connection strength defined by $|J_{ij}/h_i|$. Changes in $|J_{ij}/h_i|$ can be considered to represent the part of the changes in the connection strength beyond those explained by the modulation of the temperature.

We observed significant modulation of $|J_{ij}/h_i|$ throughout sleep in both the DMN and FPN (SWS/REM: DMN, $F_{(2,\ 262)} = 200.8/138.6$; FPN, $F_{(2,\ 218)} = 182.6/158.6$, respectively. $P < 0.01$, Friedman tests, Bonferroni-corrected, Fig. 4A). The changes in $|J_{ij}/h_i|$ were qualitatively the same as those in $|J_{ij}|$ for all the sleep types and RSNs. The values in P2 and P3 were significantly different from those in P1 (SWS/REM: DMN, $z > 9.8/5.1$; FPN, $z > 9.0/8.8$, respectively. $P < 0.01$, Wilcoxon signed rank tests, Bonferroni-corrected; Fig. 4A). The values changed monotonically mostly in P2 and reached a plateau by P3 (Fig. 4B). Furthermore, the $|J_{ij}/h_i|$ values of all the region pairs in P3 were significantly different from those in P1 for both RSNs and both sleep periods (SWS/REM: DMN, $t_{(131)} = 11.5/9.8$, $P < 1.1 \times 10^{-21}/4.1 \times 10^{-17}$; FPN, $t_{(109)} = 8.6/8.9$, $P < 5.4 \times 10^{-14}/1.6 \times 10^{-14}$, respectively. $P < 0.01$, paired t tests, Bonferroni-corrected; Fig. 4C). The $|J_{ij}/h_i|$ immediately after each sleep period was also significantly different from that in P1 ($P < 0.01$, paired t test, Bonferroni-corrected; Fig. S4). Taken together, the change in the connection strength is not entirely explained by the change in the single temperature parameter and represents essential changes in the connectivity in the RSNs.

Finally, the aforementioned modulation of the network activity could not be explained by the change in the delta power (1–4 Hz) in the EEG because the EEG spectral power did not significantly change among P1, P2, and P3 (Fig. S9).

Relationship between activity changes during SWS and REM sleep

The results obtained so far suggest that the changes in the macroscopic network activity during SWS are opposite to those that occur during REM sleep for each RSN. Therefore, the changes during REM periods are expected to be negatively correlated with those during SWS periods. We plotted the amounts of the changes (i.e., the difference between P1 and P3) in the basal brain activity (h_i), the connection strength ($|J_{ij}|$), and the normalized connection strength ($|J_{ij}/h_i|$), through SWS periods against those through REM periods (Fig. 5). At the level of each brain region and region pair, the changes through SWS periods and those through REM periods were negatively correlated in both the DMN and FPN (DMN/FPN: correlation coefficients: $r = 0.72/0.82$ for h_i, $r = 0.91/0.94$ for $|J_{ij}|$, and $r = 0.63/0.85$ for $|J_{ij}/h_i|$, respectively. $P < 0.05$, Bonferroni-corrected against types of RSN). The correlation was also significant when the amount of the activity change was redefined as the difference between pre and post SWS/REM periods, instead of that between P1 and P3 (Fig. S5).

Comparison with other methods of functional connectivity

We attempted to reproduce the present results using other methods for estimating connectivity between pairs of brain regions. To the same data set, we applied three methods: the functional connectivity on the basis of Pearson's correlation coefficient (Biswal et al., 1995; Fair et al., 2009; Greicius et al., 2004; Honey et al., 2009; Uddin et al., 2009), connection strength calculated from the partial correlation (Salvador et al., 2005, 2008), and that calculated from the mutual information (Salvador et al., 2008, 2010).

We observed moderately significant differences in the connection strength between P1 and P3 ($z > 2.2$, $P < 0.05$, Wilcoxon signed rank test, Fig. S6B) when the partial correlation method was applied. Although the results did not survive Bonferroni correction for multiple comparison, the pattern of modulation detected by the partial correlation method was consistent with that detected by the pairwise MEM. We did not observe significant differences when the other two methods were applied.

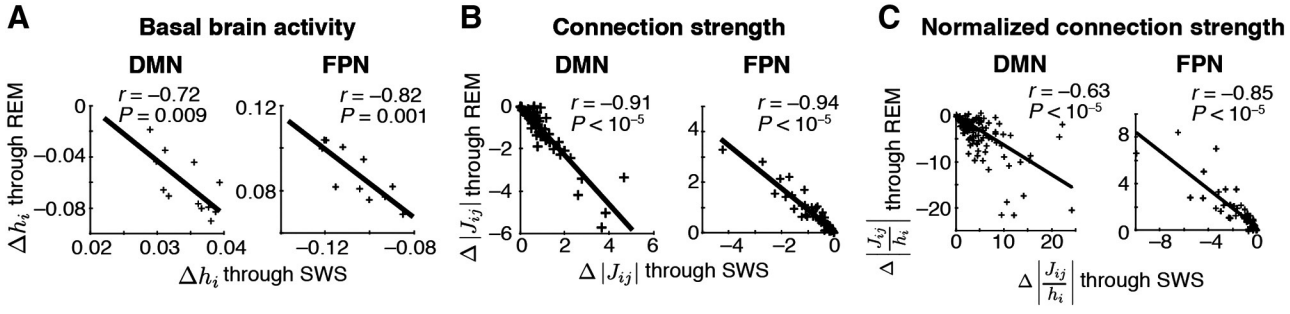

Fig. 5. Negatively correlated modulations of the network activity in SWS and REM periods. In each panel, the difference in the network activity between P3-REM and P1-REM is plotted against the difference between P3-SWS and P1-SWS. A. Results for the basal brain activity for each RSN. A cross represents the activity change at an individual brain region. The changes throughout SWS periods are negatively correlated with those throughout REM periods, as indicated by the negative values of Pearson's correlation coefficient r. Panels B and C show similar relationships in the connection strength and normalized connection strength, respectively. A cross represents the activity changes for a specific pair of regions.

Somato-sensory network – another RSN

To further support the "macroscopic network-dependent activity change" hypothesis, we examined modulation of activity of another RSN, somato-sensory network (SMN) (Fair et al., 2009). The network is considered to be relevant to early stages of perception processing (Dosenbach et al., 2006; Fair et al., 2009). Because the amount of the present data is limited, the number of the regions of interests was restricted to ten (Table S5). The network activity in the SMN altered in a manner similar to that for the FPN. In the SWS period, the basal brain activity, connection strength, and normalized connection strength at all the regions and region pairs significantly decreased ($P < 0.05$ in the Friedman test; Figs. 6A, B, and C). In particular, the values at P2 and P3 were significantly smaller than those at P1 ($P < 0.05$ in the paired t-test, Bonferroni corrected; Figs. 6A, B, and C). The opposite patterns were observed for REM sleep.

Furthermore, as observed in the DMN and FPN, the changes in the network activity throughout SWS periods were negatively correlated with those throughout REM periods at the level of each region and region pair ($r < 0.70$, $P < 0.05$; Figs. 6D, E, and F). The results on the SMN are consistent with the notion that the pattern of activity changes throughout sleep is determined by the type of RSN.

Discussion

In the present study, we showed that the network activity, quantified by the basal brain activity (i.e., h_i) and connection strength (i.e., $|J_{ij}|$), in the DMN increases during SWS periods and decreases during REM periods, whereas the network activity in the FPN and SMN changes in the opposite pattern. Moreover, in all RSNs, the activity changes during SWS periods were negatively correlated with those during REM periods. Our neuroimaging results present macroscopic evidence for network-dependent activity changes during sleep.

Previous human fMRI studies on brain activity during sleep mainly focused on the comparison across different sleep stages. For example, the DMN tends to be decoupled as the sleep stage gets deeper (Andrade et al., 2011; Horovitz et al., 2009; Sämann et al., 2011), and the FPN shows a similar tendency (Spoormaker et al., 2012). The present results are not directly comparable with these findings because we have examined changes within rather than across sleep stages. The present findings are consistent with an intra-cerebral EEG study that reported a decrease in the synaptic strength during SWS in the lateral frontal areas, some of which belong to the FPN (Nir et al., 2011).

Methodological limitations

A limitation of the present study is that we did not distinguish the SWS and REM periods observed early in the entire sleep from those observed late in the sleep. It is well known that SWS is dominant in early sleep, whereas REM sleep in late sleep (Diekelmann and Born, 2010). In addition, previous EEG studies showed that the spectral power of slow-wave activity is different between early and late sleep (Finelli et al., 2000; Tinguely et al., 2006). Therefore, network activity during SWS and REM periods in early sleep may be different from those in late sleep. We could not assess the influence of this potentially confounding factor because of the limited amount of the data. If we divide the present data into the data recorded in early sleep and those in late sleep, we do not obtain sufficiently high accuracy of fit of the pairwise MEM. Due to the same technical reason, we could not directly estimate changes in the network activity throughout the entire sleep using the pairwise MEM. Therefore, we compared the modulation in the partial correlation in the early and late nights. We found that the modulation during SWS was somewhat stronger in the early night than in the late night, whereas the modulation during REM sleep was larger in the late than early right (Fig. S8). Although these results did not survive statistical tests, they are consistent with the previous findings (Finelli et al., 2000; Tinguely et al., 2006; Diekelmann and Born, 2010).

Another limitation of the present study is the interpretation of the present findings. The results cannot be directly translated to microscopic neural mechanisms. Like other fMRI studies, our results are based on indirect recording of brain activity. It is necessary to directly confirm the present findings in future studies using, for instance, electrocorticography. The pairwise MEM is generally accurate at describing microscopic neural activity (Ganmor et al., 2011; Ohiorhenuan et al., 2010; Schneidman et al., 2006; Shlens et al., 2006; Stephens et al., 2011; Tang et al., 2008). Furthermore, the method can simultaneously quantify both local neural activity and connection strength. In contrast, except few studies (Grosmark et al., 2012), previous microscopic studies investigated either local neural activity (Chauvette et al., 2012; Dang-Vu

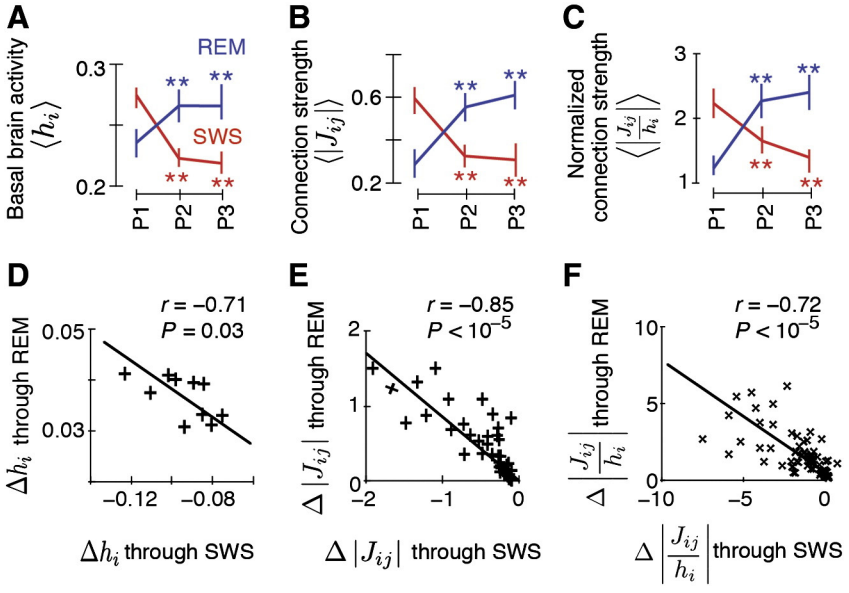

Fig. 6. Dynamics of the network activity in the SMN. A. Averaged basal brain activity. ** indicates a significant difference compared with the values at P1 ($P < 0.01$, Bonferroni-corrected). Error bar: s.d. B. Averaged connection strength. C. Average of the normalized connection strength. D. Modulations of the basal brain activity. A cross represents the activity change at an individual brain region. E. Modulations of the connection strength. A cross represents the activity changes for a pair of regions. F. Modulations of the normalized connection strength.

et al., 2008; Grosmark et al., 2012) or connection strength (Boly et al., 2012; Bushey et al., 2011; Gilestro et al., 2009; Grosmark et al., 2012; Horovitz et al., 2009; Nir et al., 2011). The pairwise MEM may be useful for revealing network-dependent activity changes during sleep on a microscopic scale.

Explanatory power of the pairwise MEM

Although previous neuroimaging studies employing the conventional method reported differences in functional connectivity between wakefulness and sleep states such as NREM sleep (Andrade et al., 2011; Horovitz et al., 2009; Koike et al., 2011; Sämann et al., 2011; Spoormaker et al., 2012), sleep stage 1 (Horovitz et al., 2008; Larson-Prior et al., 2009, 2011; Spoormaker et al., 2012; Uehara et al., 2013; van Dongen et al., 2011), SWS (Chow et al., 2013; Koike et al., 2011; Spoormaker et al., 2012), and REM sleep (Chow et al., 2013; Laureys et al., 2001; Maquet et al., 2000), they did not focus on differences in the functional connectivity within each sleep period.

In contrast, we probed the within-stage difference using the pairwise MEM to detect significant modulation in the network activity. Although there is no agreed consensus regarding the modulation in brain network activity within sleep periods, the present results provide some evidence toward understanding of this issue, and the results seem to owe much to the performance of the pairwise MEM. Unlike the correlation-based method, the pairwise MEM does not suffer from spurious correlations induced by common neighbors of two brain regions. The method based on the partial correlation (Salvador et al., 2005, 2008) was also able to detect similar patterns of modulation in the connection strength (Fig. S6B) probably for the same reason.

In some cases, all the basal brain activity values (i.e., h_i) and connection strength values (i.e., $|J_{ij}|$) simultaneously decreased toward zero during sleep. This decline does not indicate the loss of the explanatory power of the pairwise MEM throughout sleep. First, the accuracy of fit of the pairwise MEM to the data was high, irrespective of the sleep period (Table S4). This indicates by definition that the pairwise MEM, which takes into account up to the second-order interaction between brain regions, is much more accurate than the independent MEM, which neglects interactions between regions. Second, the Kullback–Leibler distance, an information-theoretic measure that quantifies the proximity between the model and the data, was roughly the same in all the periods including those in which h_i and $|J_{ij}|$ are small (Fig. S7). This result further supports that the pairwise MEM was consistently accurate throughout the experiment, whereas the recorded data were apparently nonstationary. Higher-order MEMs, which incorporate, for example, triplet interactions, are therefore unnecessary for describing the current data.

Anti-correlation between the DMN and FPN

Previous studies found anti-correlation between the DMN and FPN during sleep. One neuroimaging study showed that the anti-correlation tends to disappear as the sleep stage proceeds (Sämann et al., 2011). Another fMRI study showed the reduction in the anti-correlation during REM particularly between the posterior cingulate cortex in the DMN and the lateral parietal region in the FPN (Chow et al., 2013). However, in other fMRI studies, the anti-correlation between the core regions in the DMN and FPN was preserved during light sleep including sleep stages 1 and 2 and NREM sleep (Horovitz et al., 2008, 2009; Larson-Prior et al., 2009, 2011).

The present results support the anticorrelation during sleep. However, we must be careful in comparing the present results with the previous ones mentioned above because, different from the previous investigations, we did not directly estimate the functional connectivity between the two RSNs. To directly examine the functional connectivity by using the MEM requires a large network including the DMN and FPN as subsets, which calls for a far larger data set than that used in the present study.

Conflict of interest

The authors declare no conflict of interests.

Author contribution

T.W. and N.M. designed this research. S. Kan, T.K., M.M., and S.M. conducted imaging experiments. T.W. and N.M. analyzed the data and wrote the manuscript. S. Konishi and Y.M. discussed the results and commented on the manuscript.

Acknowledgments

We thank Drs. Kazuhiko Kume, Taira Uehara, and Taro Ueno for their valuable discussions. NM acknowledges financial supports provided through Grants-in-Aid for Scientific Research (No. 23681033) from MEXT, Japan, and the Nakajima Foundation. This work was supported by CREST of Japan Science and Technology (JST), Grant-in-Aid for Young Scientists (B) from the MEXT (No. 22700287), Society for the Promotion of Science Research Foundation for Young Scientists (222882) to TW, a Grant-in-Aid for Scientific Research B (22300134) to S.K., MEXT/JSPS KAKENHI Grant Numbers 19002010, 24220008 to YM, CREST Japan Science and Technology Agency to YM, and a grant from Takeda Science Foundation to YM.

Appendix A. Supplementary data

Supplementary data to this article can be found online at http://dx.doi.org/10.1016/j.neuroimage.2014.04.079.

References

Adachi, Y., Osada, T., Sporns, O., Watanabe, T., Matsui, T., Miyamoto, K., Miyashita, Y., 2012. Functional connectivity between anatomically unconnected areas is shaped by collective network-level effects in the macaque cortex. Cereb. Cortex 22, 1586–1592.
Andrade, K.C., Spoormaker, V.I., Dresler, M., Wehrle, R., Holsboer, F., Sämann, P.G., Czisch, M., 2011. Sleep spindles and hippocampal functional connectivity in human NREM sleep. J. Neurosci. 31, 10331–10339.
Aserinsky, E., Kleitman, N., 1953. Regularly occurring periods of eye motility, and concomitant phenomena, during sleep. Science 118, 273–274.
Behzadi, Y., Restom, K., Liau, J., Liu, T.T., 2007. A component based noise correction method (CompCor) for BOLD and perfusion based fMRI. NeuroImage 37, 90–101.
Birn, R.M., Diamond, J.B., Smith, M.A., Bandettini, P.A., 2006. Separating respiratory-variation-related fluctuations from neuronal-activity-related fluctuations in fMRI. NeuroImage 31, 1536–1548.
Biswal, B., Yetkin, F.Z., Haughton, V.M., Hyde, J.S., 1995. Functional connectivity in the motor cortex of resting human brain using echo-planar MRI. Magn. Reson. Med. 34, 537–541.
Boly, M., Perlbarg, V., Marrelec, G., Schabus, M., Laureys, S., Doyon, J., Pélégrini-Issac, M., Maquet, P., Benali, H., 2012. Hierarchical clustering of brain activity during human nonrapid eye movement sleep. Proc. Natl. Acad. Sci. U. S. A. 109, 5856–5861.
Buckner, R.L., Andrews-Hanna, J.R., Schacter, D.L., 2008. The brain's default network: anatomy, function, and relevance to disease. Ann. N. Y. Acad. Sci. 1124, 1–38.
Bushey, D., Tononi, G., Cirelli, C., 2011. Sleep and synaptic homeostasis: structural evidence in Drosophila. Science 332, 1576–1581.
Chai, X.J., Castañón, A.N., Ongür, D., Whitfield-Gabrieli, S., 2012. Anticorrelations in resting state networks without global signal regression. NeuroImage 59, 1420–1428.
Chang, C., Glover, G.H., 2009a. Relationship between respiration, end-tidal CO2, and BOLD signals in resting-state fMRI. NeuroImage 47, 1381–1393.
Chang, C., Glover, G.H., 2009b. Effects of model-based physiological noise correction on default mode network anti-correlations and correlations. NeuroImage 47, 1448–1459.
Chauvette, S., Seigneur, J., Timofeev, I., 2012. Sleep oscillations in the thalamocortical system induce long-term neuronal plasticity. Neuron 75, 1105–1113.
Chow, H.M., Horovitz, S.G., Carr, W.S., Picchioni, D., Coddington, N., Fukunaga, M., Xu, Y., Balkin, T.J., Duyn, J.H., Braun, A.R., 2013. Rhythmic alternating patterns of brain activity distinguish rapid eye movement sleep from other states of consciousness. Proc. Natl. Acad. Sci. U. S. A. 110, 10300–10305.
Cirelli, C., Tononi, G., 2008. Is sleep essential? PLoS Biol. 6, e216.
Dang-Vu, T.T., Schabus, M., Desseilles, M., Albouy, G., Boly, M., Darsaud, A., Gais, S., Rauchs, G., Sterpenich, V., Vandewalle, G., Carrier, J., Moonen, G., Balteau, E., Degueldre, C., Luxen, A., Phillips, C., Maquet, P., 2008. Spontaneous neural activity during human slow wave sleep. Proc. Natl. Acad. Sci. U. S. A. 105, 15160–15165.

Diekelmann, S., Born, J., 2010. The memory function of sleep. Nat. Rev. Neurosci. 11, 114–126.
Diekelmann, S., Büchel, C., Born, J., Rasch, B., 2011. Labile or stable: opposing consequences for memory when reactivated during waking and sleep. Nat. Neurosci. 14, 381–386.
Dosenbach, N.U.F., Visscher, K.M., Palmer, E.D., Miezin, F.M., Wenger, K.K., Kang, H.C., Burgund, E.D., Grimes, A.L., Schlaggar, B.L., Petersen, S.E., 2006. A core system for the implementation of task sets. Neuron 50, 799–812.
Fair, D.A., Cohen, A.L., Power, J.D., Dosenbach, N.U.F., Church, J.A., Miezin, F.M., Schlaggar, B.L., Petersen, S.E., 2009. Functional brain networks develop from a "local to distributed" organization. PLoS Comput. Biol. 5, e1000381.
Finelli, L.A., Baumann, H., Borbély, A.A., Achermann, P., 2000. Dual electroencephalogram markers of human sleep homeostasis: correlation between theta activity in waking and slow-wave activity in sleep. Neuroscience 101, 523–529.
Fox, M.D., Zhang, D., Snyder, A.Z., Raichle, M.E., 2009. The global signal and observed anticorrelated resting state brain networks. J. Neurophysiol. 101, 3270–3283.
Ganmor, E., Segev, R., Schneidman, E., 2011. The architecture of functional interaction networks in the retina. J. Neurosci. 31, 3044–3054.
Gilestro, G.F., Tononi, G., Cirelli, C., 2009. Widespread changes in synaptic markers as a function of sleep and wakefulness in Drosophila. Science 324, 109–112.
Greicius, M.D., Krasnow, B., Reiss, A.L., Menon, V., 2003. Functional connectivity in the resting brain: a network analysis of the default mode hypothesis. Proc. Natl. Acad. Sci. U. S. A. 100, 253–258.
Greicius, M.D., Srivastava, G., Reiss, A.L., Menon, V., 2004. Default-mode network activity distinguishes Alzheimer's disease from healthy aging: evidence from functional MRI. Proc. Natl. Acad. Sci. U. S. A. 101, 4637–4642.
Grosmark, A.D., Mizuseki, K., Pastalkova, E., Diba, K., Buzsáki, G., 2012. REM sleep reorganizes hippocampal excitability. Neuron 75, 1001–1007.
Hayasaka, S., 2013. Functional connectivity networks with and without global signal correction. Front. Hum. Neurosci. 7, 880.
Hobson, J.A., Pace-Schott, E.F., 2002. The cognitive neuroscience of sleep: neuronal systems, consciousness and learning. Nat. Rev. Neurosci. 3, 679–693.
Honey, C.J., Sporns, O., Cammoun, L., Gigandet, X., Thiran, J.P., Meuli, R., Hagmann, P., 2009. Predicting human resting-state functional connectivity from structural connectivity. Proc. Natl. Acad. Sci. U. S. A. 106, 2035–2040.
Horovitz, S.G., Fukunaga, M., de Zwart, J.A., van Gelderen, P., Fulton, S.C., Balkin, T.J., Duyn, J.H., 2008. Low frequency BOLD fluctuations during resting wakefulness and light sleep: a simultaneous EEG-fMRI study. Hum. Brain Mapp. 29, 671–682.
Horovitz, S.G., Braun, A.R., Carr, W.S., Picchioni, D., Balkin, T.J., Fukunaga, M., Duyn, J.H., 2009. Decoupling of the brain's default mode network during deep sleep. Proc. Natl. Acad. Sci. U. S. A. 106, 11376–11381.
Huber, R., Ghilardi, M.F., Massimini, M., Tononi, G., 2004. Local sleep and learning. Nature 430, 78–81.
Huber, R., Ghilardi, M.F., Massimini, M., Ferrarelli, F., Riedner, B.A., Peterson, M.J., Tononi, G., 2006. Arm immobilization causes cortical plastic changes and locally decreases sleep slow wave activity. Nat. Neurosci. 9, 1169–1176.
Ji, D., Wilson, M.A., 2007. Coordinated memory replay in the visual cortex and hippocampus during sleep. Nat. Neurosci. 10, 100–107.
Kaufmann, C., Wehrle, R., Wetter, T.C., Holsboer, F., Auer, D.P., Pollmächer, T., Czisch, M., 2006. Brain activation and hypothalamic functional connectivity during human non-rapid eye movement sleep: an EEG/fMRI study. Brain 129, 655–667.
Koike, T., Kan, S., Misaki, M., Miyauchi, S., 2011. Connectivity pattern changes in default-mode network with deep non-REM and REM sleep. Neurosci. Res. 69, 322–330.
Larson-Prior, L.J., Zempel, J.M., Nolan, T.S., Prior, F.W., Snyder, A.Z., Raichle, M.E., 2009. Cortical network functional connectivity in the descent to sleep. Proc. Natl. Acad. Sci. U. S. A. 106, 4489–4494.
Larson-Prior, L.J., Power, J.D., Vincent, J.L., Nolan, T.S., Coalson, R.S., Zempel, J., Snyder, A.Z., Schlaggar, B.L., Raichle, M.E., Petersen, S.E., 2011. Modulation of the brain's functional network architecture in the transition from wake to sleep. Prog. Brain Res. 193, 277–294.
Laureys, S., Peigneux, P., Phillips, C., Fuchs, S., Degueldre, C., Aerts, J., Del Fiore, G., Petiau, C., Luxen, A., Van Der Linden, M., Cleeremans, A., Smith, C., Maquet, P., 2001. Experience-dependent changes in cerebral functional connectivity during human rapid eye movement sleep. Neuroscience 105, 521–525.
Logothetis, N.K., Pauls, J., Augath, M., Trinath, T., Oeltermann, A., 2001. Neurophysiological investigation of the basis of the fMRI signal. Nature 412, 150–157.
Maquet, P., Laureys, S., Peigneux, P., Fuchs, S., Petiau, C., Phillips, C., Aerts, J., Del Fiore, G., Degueldre, C., Meulemans, T., Luxen, A., Franck, G., Van Der Linden, M., Smith, C., Cleeremans, A., 2000. Experience-dependent changes in cerebral activation during human REM sleep. Nat. Neurosci. 3, 831–836.
McKeown, M.J., Makeig, S., Brown, G.G., Jung, T.P., Kindermann, S.S., Bell, A.J., Sejnowski, T. J., 1998. Analysis of fMRI data by blind separation into independent spatial components. Hum. Brain Mapp. 6, 160–188.
Murphy, K., Birn, R.M., Handwerker, D.A., Jones, T.B., Bandettini, P.A., 2009. The impact of global signal regression on resting state correlations: are anti-correlated networks introduced? NeuroImage 44, 893–905.
Nir, Y., Staba, R.J., Andrillon, T., Vyazovskiy, V.V., Cirelli, C., Fried, I., Tononi, G., 2011. Regional slow waves and spindles in human sleep. Neuron 70, 153–169.
Ohiorhenuan, I.E., Mechler, F., Purpura, K.P., Schmid, A.M., Hu, Q., Victor, J.D., 2010. Sparse coding and high-order correlations in fine-scale cortical networks. Nature 466, 617–621.
Peigneux, P., Laureys, S., Fuchs, S., Collette, F., Perrin, F., Reggers, J., Phillips, C., Degueldre, C., Del Fiore, G., Aerts, J., Luxen, A., Maquet, P., 2004. Are spatial memories strengthened in the human hippocampus during slow wave sleep? Neuron 44, 535–545.
Raichle, M.E., MacLeod, A.M., Snyder, A.Z., Powers, W.J., Gusnard, D.A., Shulman, G.L., 2001. A default mode of brain function. Proc. Natl. Acad. Sci. U. S. A. 98, 676–682.
Rechtschaffen, A., Kales, A., 1968. A manual of standardized terminology, techniques and scoring system of sleep stages in human subjects, Brain Information Service/Brain Research Institute, University of California Los Angeles.
Roudi, Y., Aurell, E., Hertz, J.A., 2009. Statistical physics of pairwise probability models. Front. Comput. Neurosci. 3, 22.
Salvador, R., Suckling, J., Coleman, M.R., Pickard, J.D., Menon, D., Bullmore, E., 2005. Neurophysiological architecture of functional magnetic resonance images of human brain. Cereb. Cortex 15, 1332–1342.
Salvador, R., Martínez, A., Pomarol-Clotet, E., Gomar, J., Vila, F., Sarró, S., Capdevila, A., Bullmore, E., 2008. A simple view of the brain through a frequency-specific functional connectivity measure. NeuroImage 39, 279–289.
Salvador, R., Anguera, M., Gomar, J.J., Bullmore, E.T., Pomarol-Clotet, E., 2010. Conditional mutual information maps as descriptors of net connectivity levels in the brain. Front. Neuroinform. 4, 115.
Sämann, P.G., Wehrle, R., Hoehn, D., Spoormaker, V.I., Peters, H., Tully, C., Holsboer, F., Czisch, M., 2011. Development of the brain's default mode network from wakefulness to slow wave sleep. Cereb. Cortex 21, 2082–2093.
Schneidman, E., Berry, M.J., Segev, R., Bialek, W., 2006. Weak pairwise correlations imply strongly correlated network states in a neural population. Nature 440, 1007–1012.
Schölvinck, M.L., Leopold, D.A., Maier, A., Ye, F.Q., Duyn, J.H., 2010. Neural basis of global resting-state fMRI activity. Proc. Natl. Acad. Sci. U. S. A. 107, 10238–10243.
Shlens, J., Field, G.D., Gauthier, J.L., Grivich, M.I., Petrusca, D., Sher, A., Litke, A.M., Chichilnisky, E.J., 2006. The structure of multi-neuron firing patterns in primate retina. J. Neurosci. 26, 8254–8266.
Spoormaker, V.I., Czisch, M., Maquet, P., Jäncke, L., 2011. Large-scale functional brain networks in human non-rapid eye movement sleep: insights from combined electroencephalographic/functional magnetic resonance imaging studies. Philos. Trans. A Math. Phys. Eng. Sci. 369, 3708–3729.
Spoormaker, V.I., Gleiser, P.M., Czisch, M., 2012. Frontoparietal Connectivity and Hierarchical Structure of the Brain's Functional Network during Sleep. Front. Neurol. 3, 80.
Stephens, G.J., Osborne, L.C., Bialek, W., 2011. Searching for simplicity in the analysis of neurons and behavior. Proc. Natl. Acad. Sci. U. S. A. 108, 15565–15571.
Tang, A., Jackson, D., Hobbs, J., Chen, W., Smith, J.L., Patel, H., Prieto, A., Petrusca, D., Grivich, M.I., Sher, A., Hottowy, P., Dabrowski, W., Litke, A.M., Beggs, J.M., 2008. A maximum entropy model applied to spatial and temporal correlations from cortical networks in vitro. J. Neurosci. 28, 505–518.
Tinguely, G., Finelli, L.A., Landolt, H.-P., Borbély, A.A., Achermann, P., 2006. Functional EEG topography in sleep and waking: state-dependent and state-independent features. NeuroImage 32, 283–292.
Tononi, G., Cirelli, C., 2003. Sleep and synaptic homeostasis: a hypothesis. Brain Res. Bull. 62, 143–150.
Tononi, G., Cirelli, C., 2006. Sleep function and synaptic homeostasis. Sleep Med. Rev. 10, 49–62.
Uddin, L.Q., Kelly, A.M., Biswal, B.B., Xavier Castellanos, F., Milham, M.P., 2009. Functional connectivity of default mode network components: correlation, anticorrelation, and causality. Hum. Brain Mapp. 30, 625–637.
Uehara, T., Yamasaki, T., Okamoto, T., Koike, T., Kan, S., Miyauchi, S., Kira, J.-I., Tobimatsu, S., 2013. Efficiency of a "small-world" brain network depends on consciousness level: a resting-state fMRI study. Cereb. Cortex 24, 1529–1539.
van Dijk, K.R.A., Hedden, T., Venkataraman, A., Evans, K.C., Lazar, S.W., Buckner, R.L., 2010. Intrinsic Functional Connectivity As a Tool For Human Connectomics: Theory, Properties, and Optimization. J. Neurophysiol. 103, 297–321.
van Dongen, E.V., Takashima, A., Barth, M., Fernández, G., 2011. Functional connectivity during light sleep is correlated with memory performance for face-location associations. NeuroImage 57, 262–270.
Wang, G., Grone, B., Colas, D., Appelbaum, L., Mourrain, P., 2011. Synaptic plasticity in sleep: learning, homeostasis and disease. Trends Neurosci. 34, 452–463.
Watanabe, T., Hirose, S., Wada, H., Imai, Y., Machida, T., Shirouzu, I., Konishi, S., Miyashita, Y., Masuda, N., 2013. A pairwise maximum entropy model accurately describes resting-state human brain networks. Nat. Commun. 4, 1370.
Weissenbacher, A., Kasess, C., Gerstl, F., Lanzenberger, R., Moser, E., Windischberger, C., 2009. Correlations and anticorrelations in resting-state functional connectivity MRI: a quantitative comparison of preprocessing strategies. NeuroImage 47, 1408–1416.
Wilson, M.A., McNaughton, B.L., 1994. Reactivation of hippocampal ensemble memories during sleep. Science 265, 676–679.
Wise, R.G., Ide, K., Poulin, M.J., Tracey, I., 2004. Resting fluctuations in arterial carbon dioxide induce significant low frequency variations in BOLD signal. NeuroImage 21, 1652–1664.
Yeh, F.C., Tang, A., Hobbs, J.P., Hottowy, P., Dabrowski, W., Sher, A., Litke, A., Beggs, J.M., 2010. Maximum entropy approaches to living neural networks. Entropy 12, 89–106.